



Journal of Geophysical Research: Atmospheres

RESEARCH ARTICLE

10.1002/2014JD022530

This article is a companion to *Barnes and Houze* [2014] doi:10.1002/2014JD022241.

Kev Points:

- Mesoscale convection yields at least as much heat as isolated deep convection
- Increased stratiform rain is the primary reason for top heavy heating in active stage
- Midlevel heating is important to the MJO and its geographical variability

Correspondence to:

H. C. Barnes, hannah@atmos.washington.edu

Citation:

Barnes, H. C., M. D. Zuluaga, and R. A. Houze Jr. (2015), Latent heating characteristics of the MJO computed from TRMM Observations, *J. Geophys. Res. Atmos.*, *120*, 1322–1334, doi:10.1002/2014JD022530.

Received 2 SEP 2014 Accepted 11 JAN 2015 Accepted article online 14 JAN 2015 Published online 25 FEB 2015

Latent heating characteristics of the MJO computed from TRMM Observations

Hannah C. Barnes¹, Manuel D. Zuluaga¹, and Robert A. Houze Jr.¹

¹Department of Atmospheric Sciences, University of Washington, Seattle, Washington, USA

Abstract The Tropical Rainfall Measurement Mission's (TRMM) Spectral Latent Heating algorithm shows the contributions of different forms of convection to the latent heating profiles of the Madden-Julian Oscillation over the central Indian and West Pacific Oceans. In both oceanic regions, storms containing broad stratiform regions produce increased upper level heating during active Madden-Julian Oscillation (MJO) phases. The largest differences between the central Indian and West Pacific Ocean heating are associated with heating produced by convective elements. Examination of the most extreme forms of convection shows that mesoscale organized convection often produces at least as much latent heat as young vigorous deep convection. Heating from nonextreme (often midlevel-topped) convection is an important component of the MJO heating in both regions in all stages of the MJO. Over the central Indian Ocean the heating profile changes from having a maximum at 2 km due to nonextreme convection to a profile during the active stage that has two maxima: one at 3 km due to nonextreme convection and 6 km owing to numerous mature mesoscale storms with broad stratiform precipitation components. Over the West Pacific, the maxima at 3 and 6 km are present in all MJO stages, but the magnitude of the 6 km maximum sharply increases in the active MJO stage due to an increase in the number of storms with broad stratiform precipitation areas.

1. Introduction

The Madden-Julian Oscillation (MJO) is the dominant source of intraseasonal (30-60 day) variability within the equatorial belt [Madden and Julian, 1971, 1972]. Convection directly associated with the MJO initiates in the western equatorial Indian Ocean, propagates along the equator, and dissipates near the dateline. This period of enhanced convective activity is referred to as the active stage of the MJO and is characterized by deep convective systems, some of which are organized on the mesoscale with large regions of stratiform precipitation. The suppressed stage of the MJO is characterized by shallower, less organized convection. The MJO is also associated with upper level circulation anomalies and teleconnections that impact weather throughout the globe [Zhanq, 2005, 2013]. Despite over four decades of research, operational models that use standard cumulus parameterizations continue to struggle to predict the MJO beyond 15 days [e.g., Waliser et al., 2003; Kerns and Chen, 2014; Ling et al., 2014]. This limited predictability is a problem because the MJO's 30-60 day period significantly impacts global weather patterns. Several studies have suggested that a major limitation to MJO prediction is inaccurate representation of convection and its multiscale interactions by cumulus parameterization schemes [e.g., Tokioka et al., 1988; Maloney and Hartmann, 2000; Wang, 2005]. Thus, improving model parameterization may enable accurate MJO forecasts to help resolve the gap between weather and climate prediction [Waliser, 2005]. However, studies provide conflicting results regarding which changes in the cumulus parameterization schemes elicit the best MJO simulations [e.g., Slingo et al., 1996; Lin et al., 2004]. Fu and Wang [2009] suggest that these diverse and sometimes conflicting results underscore the need for more reliable observations to validate simulations; i.e., the first step toward improving MJO prediction involves the analysis of observational data indicating the behavior of the cloud population and its impacts.

One of the primary ways that convection influences the general circulation is through the release of latent heat. Thus, numerous modeling and observational studies have investigated the variability of latent heating during the MJO. Stratiform precipitation is associated with a top heavy latent heating profile with heating aloft and cooling below the melting level and was shown by *Hartmann et al.* [1984] and *Schumacher et al.* [2004] to significantly impact the atmospheric circulation. However, even though stratiform precipitation is one of most variable components of the cloud population during the MJO [e.g., *Barnes and Houze*, 2013], deep stratiform heating alone is not capable of producing accurate MJO simulations [e.g., *Fu and Wang*, 2009; *Li et al.*, 2009]. Recently, it has been suggested that a transition from



shallow heating in the suppressed stage to deep heating in the active stage is an important component in accurate MJO simulations [e.g., Zhang and Mu, 2005; Fu and Wang, 2009; Li et al., 2009; Jiang et al., 2011]. Additionally, Lappen and Schumacher [2012] showed that skillful MJO simulations not only require accurate vertical profiles of latent heating, but accurate horizontal distributions of latent heating were also important. As modeling studies increasingly indicate that the accuracy of MJO simulations is highly sensitive to the distribution of latent heating, increasingly detailed observations of latent heating are required.

The transition from shallow to deep heating is captured in observational studies that derive latent heating from rawinsonde networks [e.g., Lin et al., 2004; Haertel et al., 2008], International Satellite Cloud Classification Project data [Jakob and Schumacher, 2008; Stachnik et al., 2013], and Tropical Rainfall Measurement Mission (TRMM) data [e.g., Morita et al., 2006; Lau and Wu, 2010; Zuluaga et al., 2010]. While latent heating is routinely derived using ground-based measurements, the spatial and temporal resolution of the data is limited since it must be derived from high-resolution thermodynamic data about the cloud population. The TRMM satellite provides a unique opportunity to investigate latent heating in the tropics since it provides over 15 years of tropics-wide high-resolution, three-dimensional data about the precipitating cloud population. However, one limitation of the previous TRMM-based latent heating studies is that they primarily analyze latent heating during the MJO as a function of height [Morita et al., 2006; Lau and Wu, 2010; Zuluaga et al., 2010]. Houze [1982, 1989] indicated that the convective and stratiform portion of storms produce distinctly different latent heating profiles. Hartmann et al. [1984] and Schumacher et al. [2004] found that, as a result of this difference, the net heating profile of a cloud population is sensitive to the fraction of convective and stratiform heating. Thus, studies that consider latent heating only as a function of height may be unable to fully explore the relationship between the cloud population and latent heating. The benefit of the TRMM Precipitation Radar (TRMM PR) is that it provides information about the nature of convective populations across the tropics. Barnes and Houze [2013] used TRMM PR observations to show the composition of the precipitating cloud population during different phases of the MJO in terms of isolated shallow convection, deep convection, and mesoscale entities including those containing stratiform rain areas. They further showed how the composition of the cloud population varied between the central Indian and West Pacific Oceans. The current study expands upon Barnes and Houze [2013] by investigating how these cloud populations with distinctly different dynamical characteristics contribute to the net latent heating observed during the MJO in the central Indian and West Pacific Oceans.

2. Methodology

The precipitating cloud systems analyzed in this study occurred from October to February 1998–2012 in the central Indian (60°-90°E, 10°S-10°N) and West Pacific (156°-170°E, 10°S-0°) Oceans. A smaller geographic region is analyzed in the West Pacific Ocean than in the Indian Ocean since Barnes and Houze [2013] showed that the variability of the cloud population is consistent across the entire central Indian Ocean domain but is distinctly different in three subregions of the West Pacific Ocean. The current study only presents results between 156°-170°E and 10°S-0° since the variability of the cloud population in this region was found by Barnes and Houze [2013] to have the most distinct peaks in deep and mesoscale convection. In this study, we use the criteria for defining categories of radar echoes that were used by Barnes and Houze [2013] to classify oceanic convection. We have not included the Maritime Continent in this study due to the complex juxtaposition of small land and ocean areas. Land-based convection tends to be more intense, which requires different reflectivity threshold criteria than those used by Barnes and Houze [2013]. Criteria applied to TRMM PR data over continental land areas use higher thresholds of intensity, echo height, and echo area [e.g., Houze et al., 2007; Romatschke et al., 2010; Romatschke and Houze, 2010; Rasmussen and Houze, 2011]. When we apply such criteria over the ocean, too much convection is filtered out of the analysis. It is unclear at this juncture how to categorize convection occurring over the complex of land, sea, and coastal environments of the Maritime Continent. By focusing on the two uniform ocean areas, we are able to use a single consistent set of criteria to categorize convection in the two regions. These two regions are meaningful to compare because the Indian Ocean region represents the upstream region of initiation of the MJO disturbance, while the West Pacific region that we have selected represents the MJO convective population in its downstream mature eastward propagating stage.

We focused on boreal fall/winter since that is the climatological peak of the MJO. One method used to track and assess the strength of the MJO is the real-time multivariate index (RMM) [Wheeler and Hendon, 2004].



To ensure that only robust MJO events are analyzed, we only consider days whose RMM magnitude is greater than one. Based on results from *Barnes and Houze* [2013], the suppressed stage in the central Indian Ocean is represented by phase 6, the transition to the active stage is represented by phase 8, the active stage is described by phase 2, and the transition to the suppressed stage is represented by phase 4. In the West Pacific, the suppressed stage is represented by phase 2, the transition to the active stage is represented by phase 4, the active stage is described by phase 6, and the transition to the suppressed stage is described by phase 8. The RMM index has some flaws. For example, *Roundy et al.* [2009] showed that the RMM index can be contaminated by Kelvin wave activity, and *Straub* [2013] demonstrated that the index may not adequately capture MJO initiation. However, *Straub* [2013] also suggests that the RMM index may adequately capture mature MJO events. Thus, given that this study analyzes long-term trends in robust MJO events in boreal winter, we expect that the flaws in the RMM index likely have a minimal impact on our results.

The current study identifies and classifies radar echoes using the methodology introduced by Houze et al. [2007] in the form modified by Barnes and Houze [2013]. We first isolate all 3-D contiguous nonzero reflectivity echoes using TRMM 2A25 version 7 data. Each 3-D echo is defined as a "storm." By basing our analysis on coherent 3-D echo structures rather than individual TRMM pixels, we are able to ensure that all of our statistics are directly associated with volumetric elements of storms that have specific dynamical characteristics and are representative of one type of member of the overall precipitating cloud population. In order to identify and isolate distinct dynamical processes within these storms, we separate the storms into their convective and stratiform portions. Then, if the stratiform portion of a storm is contiguous over at least 50,000 km², that stratiform portion is referred to as a broad stratiform region (BSR). If the convective portion of the storm has a contiguous region of 30 dBZ echo covering at least 800 km², that convective portion is referred to as a wide convective core (WCC). If the convective portion of the storm has a contiguous region of 30 dBZ echo that extends above 8 km and covers less than 800 km², that convective region is called a deep convective core (DCC). Convective core that has a contiguous region of 30 dBZ echo that covers more than 800 km² and extends above a height of 8 km is classified only as a WCC. Zuluaga and Houze [2013] analyzed these same echo features and found that DCC is associated with recently formed mesoscale convective systems (MCSs) [Houze, 2004], WCC is associated with mature MCSs, and BSR is associated with late stage, dissipating MCSs.

Schumacher and Houze [2003] and Zuluaga and Houze [2013] identified isolated shallow echoes (ISE) to represent the smaller precipitating convective elements in an ensemble of clouds. We also identify this category, defined as having echo top heights at most 1 km below the melting level and separate from deeper convection. Although the identified elements in this category represent a significant part of the population of convective elements studied here [e.g., Barnes and Houze, 2013], the full impact of the shallow and/or nonprecipitating convection on the latent heating variability associated with the MJO will likely be underestimated in this study since the TRMM PR has a sensitivity of ~17 dBZ.

It is important to note that echo features labeled BSR, WCC, or DCC are elements that are embedded within a three-dimensional echo entity that we label as a storm. (i.e., BSRs, WCCs, and DCCs are small features always embedded within a larger storm). In the analysis that follows, we will first determine the net latent heating associated only with the echo features BSR, WCC, DCC, and ISE. Then we will determine the net heating by the storms containing these echo features.

Storms sometimes contain more than one type of intense echo at the same time. To avoid multiple counting of storms with intense elements, it is necessary to classify storms containing DCC, WCC, and/or BSR in a hierarchal manner. First, any storm containing a BSR is automatically classified as a storm containing a broad stratiform region (S-BSR). S-BSRs always contain a BSR and may or may not contain a DCC and/or WCC. Then, any storm lacking a BSR but containing a WCC is classified as a storm containing a wide convective core (S-WCC). S-WCC always contains WCC, never contains BSR, and may or may not contain DCCs. Finally, any storm containing only a DCC is classified as a storm containing a deep convective core (S-DCC). S-DCC always contains DCC and never contains WCCs or BSRs. By defining the S-DCCs, S-WCCs, and S-BSRs, in this hierarchal manner we ensure that each storm containing at least one DCC, WCC, and/or BSR is included in our analysis only once. While BSR, WCC, and DCC entities only contain stratiform or convective echoes, the storms containing these echo features (i.e., S-BSR, S-WCC, and S-DCC) can be composed of a mixture of convective and stratiform echoes and lighter precipitation not classified in any of those two categories. Any 3-D contiguous storm that does not satisfy as S-DCC, S-WCC, or S-BSR is referred to as a nonclassified storm (S-Non). The term S-All represents all of the "storms" combined.



Latent heating data used in this study is given by the TRMM 2H25 product, which provides 19 vertical levels of latent heating data derived using the Spectral Latent Heating algorithm (SLH) at each orbital grid point along the TRMM PR's swath. The SLH calculates latent heating from three lookup tables generated from a cloud-resolving simulation of convection during the Tropical Ocean Global Atmosphere Coupled Ocean Atmosphere Response Experiment (TOGA COARE) [Shige et al., 2004, 2007, 2009]. Data from the TRMM PR is used to select the appropriate profile from these lookup tables. To provide a measure of the net latent heating associated with each storm, the 2H25 data are mapped onto the same Cartesian grid as the 2A25 reflectivity data and summed over all grid points within the storm. The net latent heating is then normalized by the number of pixels sensed by the TRMM PR, which accounts for the different sample size in each geographic region and MJO phase.

The SLH algorithm is not the only TRMM-based product that derives latent heating profiles. For example, the convective-stratiform heating (CSH) algorithm uses TRMM PR and TRMM microwave imager data to derive profiles using lookup tables generated from cloud-resolving simulations of convection observed during numerous field campaigns throughout the globe [Tao et al., 1993, 2006, 2010]. Additionally, for local shortterm field projects, latent heating can be derived from rawinsonde data and reanalyses. The lookup tables and ~17 dBZ sensitivity of the TRMM PR are the primary shortcomings of the SLH algorithm. Previous studies have compared the latent heating derived using the SLH algorithm with heating derived from other TRMMbased algorithms, reanalyses, and rawinsonde budgets and identified differences in the methods, particularly in terms of the structure and magnitude of low-level heating [e.g., Tao et al., 2006; Hagos et al., 2010; Zhang et al., 2010; Ling and Zhang, 2011; Jiang et al., 2011]. The SLH algorithm tends to produce more shallow heating than the other TRMM algorithms. Additionally, while the SLH profile tends peak twice, once at low levels and once at upper levels, other data sources sometimes only contain one peak at mid-upper levels. Given that latent heating is a variable that is derived using numerical simulations and/or lookup tables, the magnitude of low-level heating is uncertain [Ling and Zhang, 2011]. For these reasons, the results of the present study must be considered with caution when analyzing shallow heating signatures derived from the SLH.

3. Latent Heating in Convective Cores, Broad Stratiform Regions, and Shallow, Isolated Echoes

Figure 1 shows the net heating profile associated with DCC, WCC, BSR, and ISE in the central Indian Ocean during the suppressed, active, and transition phases of MJO. Only the magnitude the net heating varies during the MJO. It should be noted that, as discussed in section 2, the profiles designated as DCC, WCC, and BSR are only for the embedded subregions of echoes that have been designated as having the extreme properties defining these features. The heating profiles of entire storms containing these types of embedded entities will be considered in section 4. The shapes of these profiles are unchanged throughout the MJO. BSRs are always associated with heating aloft and cooling below. DCCs and WCCs are characterized by deep heating. ISEs have a characteristic peak in heating near the surface. These heating structures are consistent with the canonical stratiform and convective heating profiles described in Houze [1982, 1989]. The net heating associated with BSR, DCC, and WCC maximizes in the active stage (Figure 1c) and minimizes during the suppressed stage (Figure 1a). While ISEs, DCCs, and WCCs produce similar amounts of latent heat as the MJO transitions into its active and suppressed stages, BSRs produce more heat when the MJO is transitioning into its active stage (Figure 1b) than when the MJO is transitioning into its suppressed stage (Figure 1d). ISEs produce slightly more net heating in the suppressed and transition stages than the active stage possibly since these elements are least common during the active stage of the MJO [Barnes and Houze, 2013]. During all stages of the MJO, even though DCC and WCC are both intense convective features, WCC consistently produce more latent heat that DCC because of their larger area coverage. Thus, WCCs indicate that mature convection that has aggregated to a more organized state contributes more to the total latent heating in the central Indian Ocean than does young, deep convection. Among the four types of echo features, BSR heating undergoes the greatest variation as a function of MJO phase. These patterns of variability are consistent with the variability of the net areal coverage of the echo features, as analyzed by Barnes and Houze [2013], not by the current numbers of features of a given type.

The shape and variability of the latent heating profile from phase to phase of the MJO are similar in the West Pacific region to those over the central Indian Ocean (Figure 2). The only notable differences between the

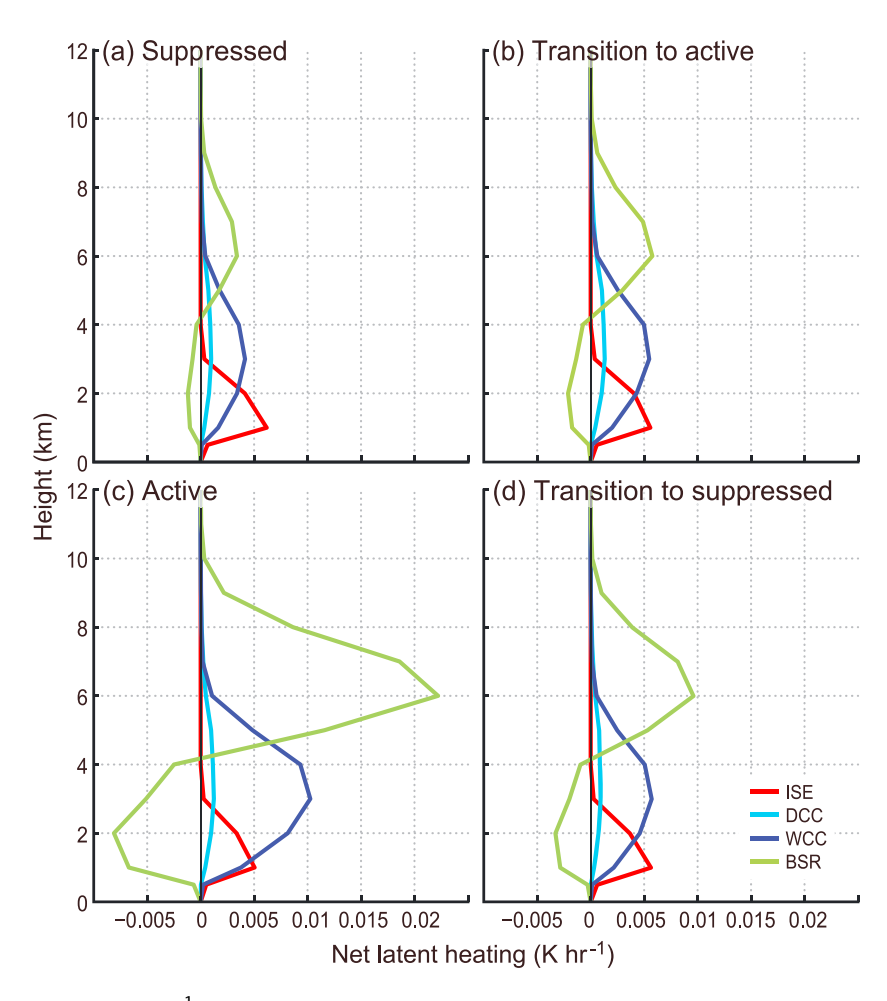


Figure 1. (a) Net heating (K/h^{-1}) from ISE (red), DCC (cyan), WCC (dark blue), and BSR (green) during the suppressed stage (phase 6) in the central Indian Ocean. Net heating is normalized by the total number of pixels sensed by the TRMM PR. (b) Same as Figure 1a except for the transition to the active stage (phase 8). (c) Same as Figure 1a except for the active stage (phase 2). (d) Same as Figure 1a except for transition to the suppressed stage (phase 4).

regions are associated with heating from BSRs. During all stages of the MJO, BSRs contribute more latent heat above 5 km in the West Pacific Ocean than in the central Indian Ocean. Additionally, the BSRs produce more heat as the MJO transitions to its suppressed stage than when the MJO transitions to its active stage, which is opposite the central Indian Ocean.

4. Contribution From Storms Containing Intense Echoes to Net Observed Latent Heating in the Central Indian Ocean

More important than the contribution of heating by the embedded entities alone is the contribution by the entire storm containing each echo core. The solid black lines in Figures 3a, 3b, 3d, and 3e show the net heating from all storms (S-All) during each stage of the MJO in the central Indian Ocean, and the total rain rate from S-All is listed in the lower right-hand side, both of which are normalized by the total number of TRMM pixels detected. The dashed and colored lines in Figure 3 show the net heating from storms designated as S-Non, S-BSR, S-WCC, S-DCC, and ISE. Given that S-All includes S-DCC, S-WCC, S-BSR, S-Non, and ISE, comparing the solid black line to the dashed and colored lines allows us to understand how storms with these different types of convective and stratiform elements contribute to the net heating profile of S-All. Unlike the DCCs, WCCs, and BSRs discussed above, S-DCCs, S-WCCs, and S-BSRs contain various combinations of convective and stratiform echoes and consistent of different mixtures of extreme and nonextreme echo subfeatures. Therefore, the latent heating profiles of DCCs, WCCs, and BSRs in Figure 1 differ from the profiles

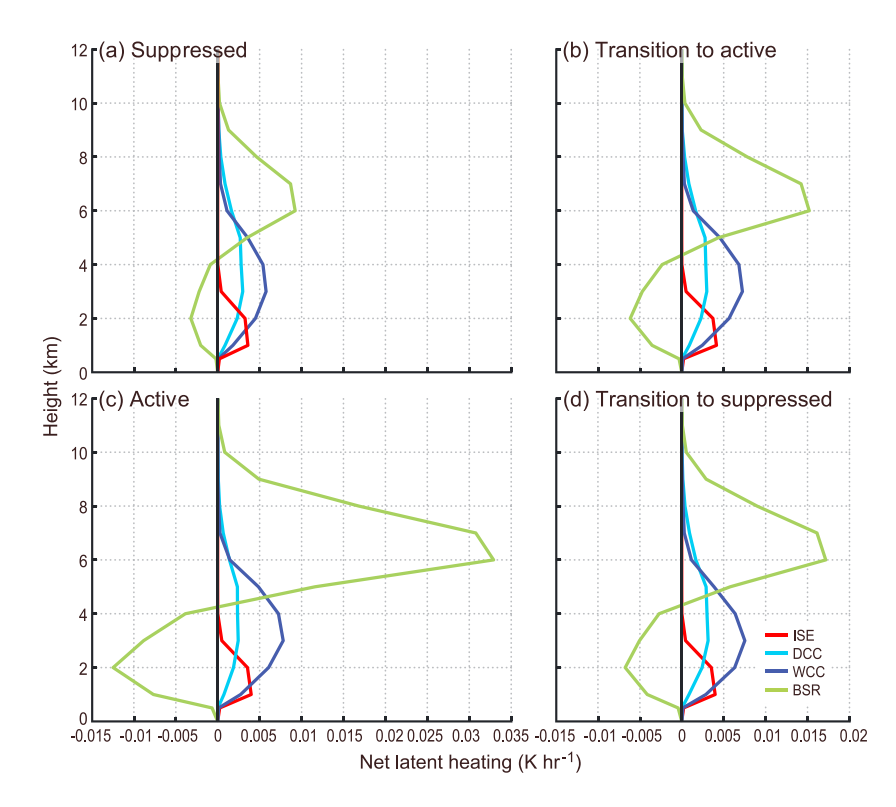


Figure 2. Same as Figure 1 except for the West Pacific with the suppressed stage represented by phase 2, the transition to the active stage presented by phase 4, the active stage represented by phase 6, and the transition to the suppressed stage by phase 8.

of S-DCCs, S-WCCs, and S-BSRs shown in Figure 3. The largest differences in the vertical profiles of heating are observed between BSR (Figure 1) and S-BSR (Figure 3). S-BSRs are characterized by substantially less low-level cooling since low-level heating associated with the convective portions of S-BSRs will partially offset the low-level cooling observed in the BSR region, which only contains stratiform echoes.

During the suppressed stage of the MJO in the central Indian Ocean, the net heating from S-All (black line in Figure 3a) maximizes near 2 km and steadily declines with height. Recall that the SLH produces similar amounts of deep heating when compared to reanalysis data or other TRMM algorithms but tends to produce more low-level heating [e.g., Hagos et al., 2010; Zhang et al., 2010; Ling and Zhang, 2011]. Thus, we are confident that the minimal upper level heating during the suppressed stage is a robust signature of the MJO, but the amplitude of maximum low-level heating may be too large. At all levels, S-Non is the dominant source of latent heating; i.e., nonextreme clouds of medium height and intensity dominate the heating profile. The profile for S-BSR is almost nonexistent. S-WCC and S-DCC contribute relatively little to the net latent heating produced by S-All. However, S-WCC contributes more to the net latent heating than the other intense echo categories, which emphasizes that even in suppressed periods organized mesoscale convection is important in the net latent heating budget. ISE convection contributes very little to the net heating; however, the TRMM PR sensitivity of ~17 dBZ precludes us from determining the full magnitude of lightly precipitating and nonprecipitating convection.

While latent heating increases at all levels as the MJO transitions into its active stage, the greatest increase occurs at upper levels. Comparing S-All in Figures 3a and 3b indicates that heating at 6 km increases by approximately $0.02\,\mathrm{K\,h^{-1}}$ during this time but heating near 2 km only increases by $0.01\,\mathrm{K\,h^{-1}}$. S-Non continues to be the dominant source of latent heat at all levels. While there is little change in the contribution by ISE and S-DCC, S-WCC and S-BSR contribute substantially more latent heat as the MJO transitions to its active stage, especially above 4 km. Associated with this increase in latent heat is an increase in the normalized rain rates, which indicates that the cloud population is beginning to become more disturbed.

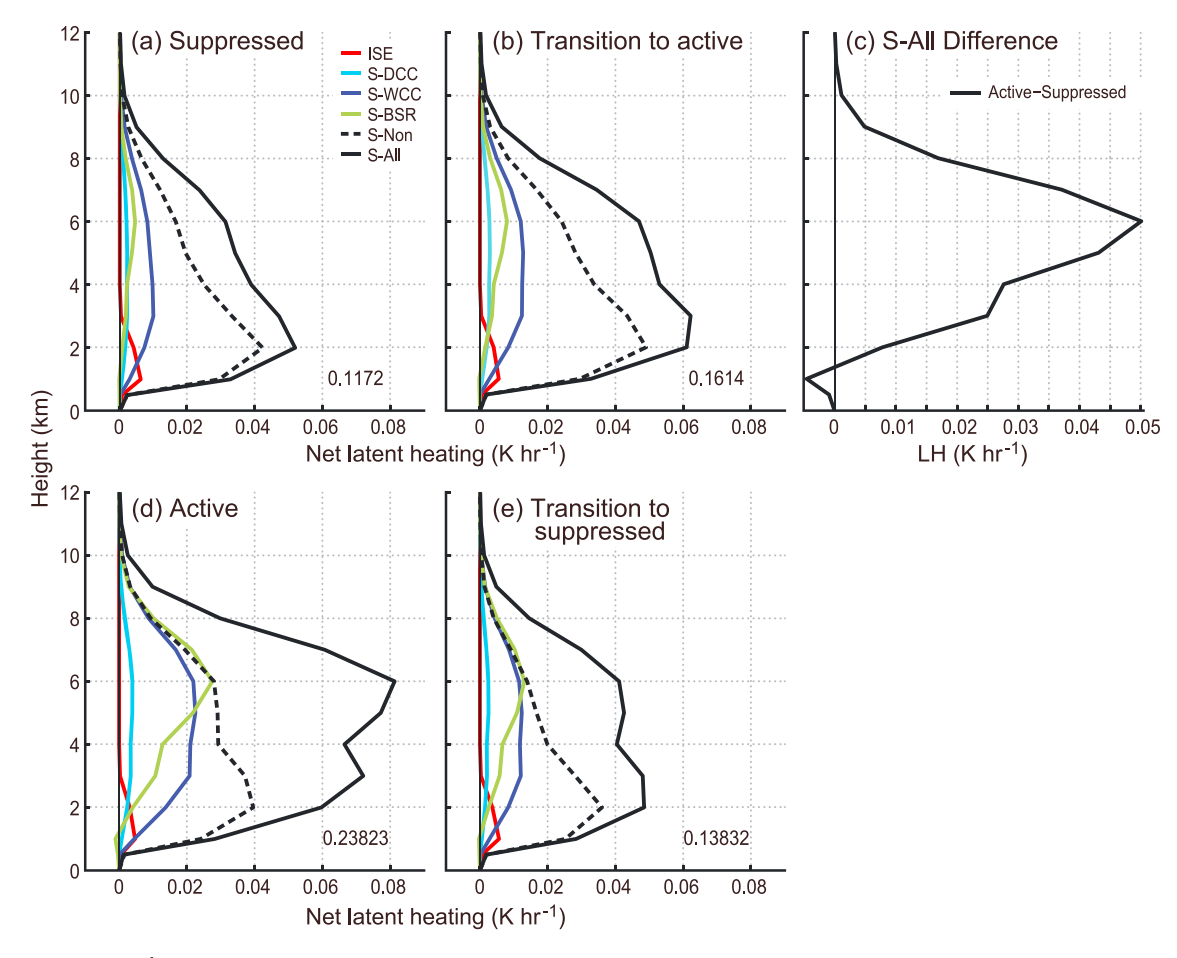


Figure 3. (a) Net heating (K h⁻¹) from ISE (red), S-DCC (cyan), S-WCC (dark blue), and S-BSR (green) during the suppressed stage (phase 6) in the central Indian Ocean. Net heating is normalized by the total number of pixels sensed by the TRMM PR. The rain rate during the suppressed stage that (phase 6) is listed in the lower right-hand side is normalized by the number of pixels sensed by the TRMM PR. (b) Same as Figure 3a except for the transition to the active stage (phase 8). (c) Difference in S-All between the active stage (phase 3) and the suppressed stage (phase 6) of the MJO. (d) Same as Figure 3a except for the active stage (phase 2). (e) Same as Figure 3a except for transition to the suppressed stage (phase 4).

During the active stage, the relative importance of heating from S-BSR and S-WCC drastically changes. The black line in Figure 3d shows that the net heating profile from S-All now has two distinct peaks, near 3 and 6 km. This dual-peak structure is a feature commonly observed in the SLH data but is sometimes absent from reanalysis and rawinsonde budgets [e.g., Hagos et al., 2010; Zhang et al., 2010]. The lower peak is associated with heating contributed by convective elements including ISE, S-DCC, S-WCC, and S-Non, which is consistent with Houze [1982, 1989]. While S-Non continues to contribute most of the heating below 5 km, the contribution by S-WCC and S-DCC substantially increases at these levels. ISEs continue to contribute very little to the net heating, although nonprecipitating or lightly precipitating convective clouds might be contributing significantly but are undetected due to the limited sensitivity of the TRMM PR. The upper level peak occurs primarily because the convection takes on mesoscale organization during active phases, and heating from S-BSR and S-WCC therefore increases. During active phases, S-BSR and S-WCC become the primary components of the S-All profile above 5 km. The contribution of heating from S-BSRs increases the most, reflecting the significant increase in occurrence of BSRs elements during the active phase [Barnes and Houze, 2013]. This drastic increase in stratiform heating during the active stage is isolated in Figure 3c, which shows the difference in the heating profile of S-All between the active and suppressed stage. The upper level heating and low-level cooling observed in this difference profile is indicative of an increase in stratiform heating during the active stage of the MJO. Additionally, given that the difference profile is strongly positive between 2 and 5 km, these results indicate that the MJO also substantially increases midlevel heating during the active stage. S-WCC continues to contribute significantly more latent heat than



S-DCC. While S-BSR, S-WCC, and S-DCC do not contain the heating by all members of the cloud population, these categories capture a significant portion of the net heating produced by S-All during the active phase and emphasize the increased roles of deep and organized convection in the population in active stages of the MJO.

The reduction in net latent heating that occurs as the MJO transitions into its suppressed stage is accompanied by a change in the vertical distribution of heating. The upper level heating maximum sharply decreases as the MJO transitions to its suppressed stage (Figure 3e) and is all but gone by the suppressed stage (Figure 3a). This decrease at upper levels is mainly attributable to less heating from S-BSRs and S-Non. The S-Non cases include mesoscale convective systems with stratiform regions that are not robust enough to qualify as BSRs but are nevertheless large enough to have an impact on the net heating profiles. While the contribution from S-WCCs is also reduced, heating from S-WCCs only decreases by 0.01 K h^{-1} while heating from S-BSR and S-Non decreased by nearly 0.02 K h^{-1} . Significant changes in the contribution by S-DCC and ISE are not observed.

Interestingly, the heating profiles during the two transition periods (Figures 3b and 3e) are distinctly different. First, the magnitude of the net heating profile for all storms (S-All) is larger as the MJO is transitioning into its active stage (Figure 3b) than when the MJO transitions to its suppressed stage (Figure 3e) at all levels. Additionally, while S-Non dominates the heating profile below 5 km during both time periods, the relative contributions of S-WCC, S-BSR, and S-Non above 5 km are notably different. When the MJO transitions into its active stage S-Non heating (nonextreme convection) is the dominant source of upper level heat. This contrasts with the transition to the suppressed stage, when S-Non, S-BSR, and S-WCC contribute equally to the upper level heating. Thus, differences in the composition of the cloud population cause the two transition periods to have dissimilar heating profiles. We conclude that during the buildup to the active phase, the population has not yet developed a strong capacity for its members to have mesoscale organization, whereas during the transition from active to suppressed stages the ability of convective elements to be organized on the mesoscale remains but the organized elements are diminishing in number.

5. Similarities and Differences Between the Central Indian and West Pacific Oceans

The black lines Figures 4a, 4b, 4d, and 4e show the net heating profiles for all storms (S-All) as the MJO propagates through the West Pacific Ocean. The colored and dashed lines in this figure indicate how ISE, S-DCC, S-WCC, S-BSR, and S-Non contribute to the S-All heating profile. Comparing Figures 3 and 4 allows us to investigate how the heating associated with the MJO differs in the central Indian and West Pacific Oceans.

There are a few similarities among the latent heating profiles observed in the central Indian and West Pacific Oceans in terms of the overall variability as the MJO propagates through these regions. First, both geographic regions are characterized by an increase in upper level heating during the active stage of the MJO. Such an increase is expected given that the active stage is characterized by an increase of deep convective activity [e.g., *Lin et al.*, 2004]. More importantly, heating associated with mature mesoscale convective systems (as indicated by increased S-BSR occurrence) varies the most and maximizes during the active stage in both regions, consistent with the maximum occurrence of BSRs during the active stages [*Barnes and Houze*, 2013]. During all stages of the MJO, S-Non is the dominant source of heat below 5 km in both regions, suggesting that convective clouds of moderate top height are an important source of heat. ISEs never contribute a substantial amount of latent heat in either region; however, nonprecipitating and lightly precipitating clouds are not seen by the TRMM PR, and they might contribute significantly to heating at low levels.

Even though both geographic regions are characterized by an increase in upper level heating during the active stage of the MJO, important differences exist between the regions in terms of the shape of the heating profile and its variability during the MJO. The heating profile associated with all storms (S-All) contains two peaks, near 3 and 6 km, during most stages of the MJO in the West Pacific Ocean (Figure 4). This dual peaked structure is only present during the active stage in the central Indian Ocean (Figure 3), which suggests that the convective population in the West Pacific Ocean contains a larger amount of deep convection than the central Indian Ocean, especially during the suppressed and transition stages of the MJO. This conclusion is further supported by the normalized rain rates, which are larger in the West Pacific than central Indian Ocean during suppressed and transition stages. Figure 4c shows the difference between the S-All profiles during the active and suppressed stages in the West Pacific Ocean. Between 2

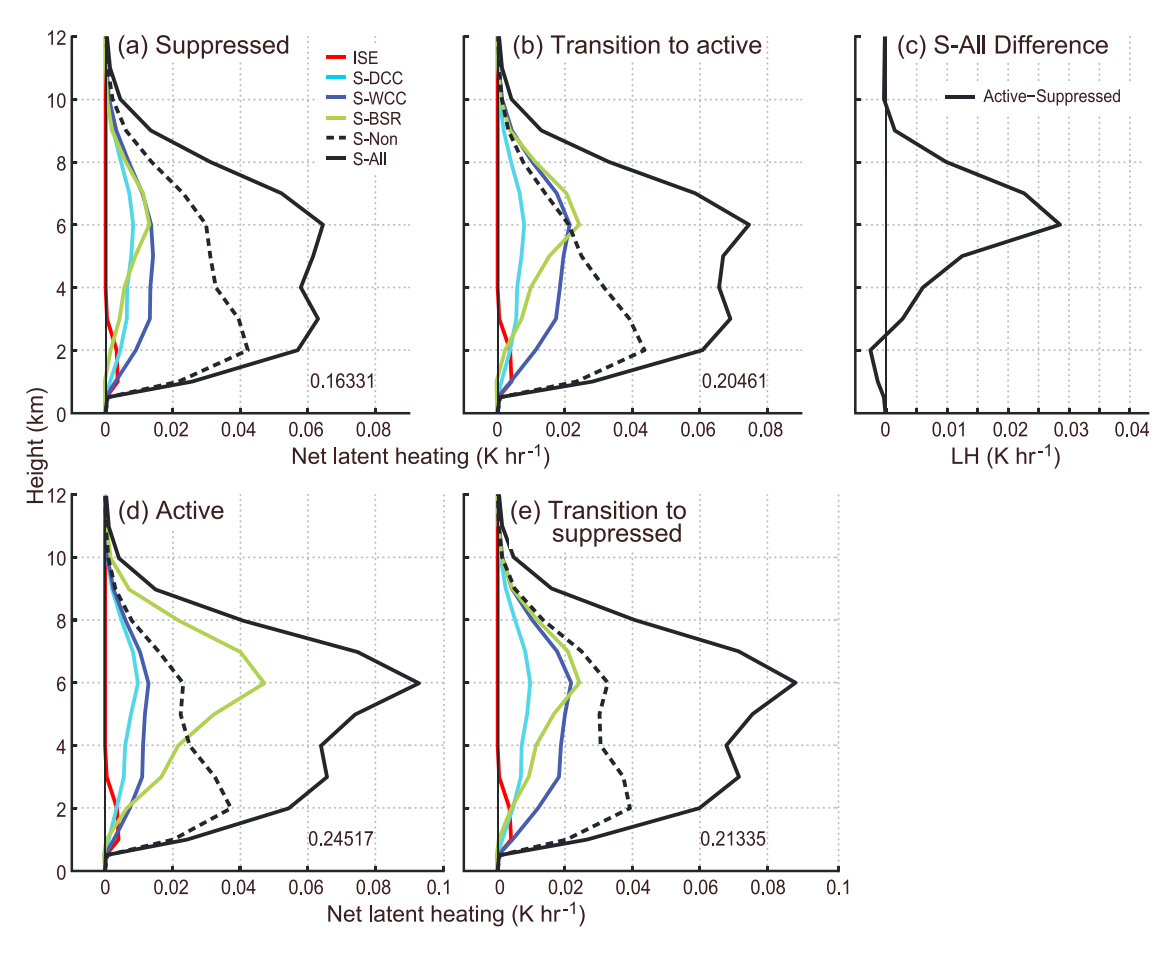


Figure 4. Same as Figure 3 except for the West Pacific with the suppressed stage represented by phase 2, the transition to the active stage presented by phase 4, the active stage represented by phase 6, and the transition to the suppressed stage by phase 8.

and 4 km the difference profile is nearly zero, which suggests that the MJO causes only minimal changes in the midlevel heating. On the other hand, the difference profile in the central Indian Ocean (Figure 3c) is strongly positive between 2 and 4 km, suggesting that the MJO strongly modifies midlevel heating in the central Indian Ocean but not in the West Pacific Ocean. Additionally, while the S-All latent heating profile in the central Indian Ocean systematically transitions from bottom heavy during the suppressed stage to top heavy during the active stage (Figure 3), the S-All heating profile in the West Pacific Ocean transitions from middle heavy during the suppressed stage to top heavy during the active stage (Figure 4). This result is further evidence that heating by moderate convection is always an important component of the net heating profile during the MJO, but the character of heating at midlevels varies between the central Indian Ocean, which is the region of MJO initiation, and the West Pacific, which is a throughway for the fully formed MJO. Furthermore, while the S-All profile indicates that more upper level heating occurs in West Pacific Ocean during its transition to the suppressed stage than during its transition to its active stage, the opposite trend is observed in the central Indian Ocean.

To gain insight into which aspects of the cloud population are responsible for these geographic differences in S-All, we consider the contribution from S-Non, S-BSR, S-WCC, and S-DCC in each region. Below 4 km, the magnitude difference between the S-Non profile and S-All profile in the central Indian Ocean (Figures 3a, 4b, 4d, and 4e) is nearly half as large as the difference in the West Pacific Ocean (Figures 4a, 4b, 4d, and 4e), suggesting that nondescript clouds of medium height and intensity have a more dominant role in heating the lower atmosphere in the central Indian Ocean, where the MJO initiates, than in the West Pacific Ocean, where the fully developed MJO propagates. Above 6 km, the S-Non profile in the West Pacific Ocean often has a secondary peak (Figures 4a, 4b, 4d, and 4e). This secondary S-Non peak is most notable in the central



Indian Ocean region during the active stage (Figure 3d) and is nearly absent in suppressed periods, suggesting that smaller regions of stratiform precipitation, which do not satisfy our S-BSR thresholds, often contribute more latent heat in the West Pacific Ocean than central Indian Ocean. Combining these results suggests that the convective population in the West Pacific Ocean is somewhat deeper and more organized than the convective population in the central Indian Ocean.

The contributions by S-BSRs, S-WCCs, and S-DCCs to S-All differ in each geographic region. While the latent heating associated with S-BSRs is always the most variable component of heating budget analyzed in this study, their contribution relative to S-DCC, S-WCC, and S-Non during the active stage in each region is notably different. Figure 4d indicates that S-BSRs dominate the latent heating above 4 km over the West Pacific Ocean during the active stage. In contrast, Figure 3d indicates that S-BSR, S-WCC, and S-Non contribute equally to the heating above 6 km in the central Indian Ocean region during the active stage. The primary difference between the central Indian and West Pacific Oceans is in the contributions from the intense convective categories S-DCC and S-WCC. While S-WCC in the West Pacific Ocean contributes substantially more latent heat during the transition stages than S-DCC, S-DCC and S-WCC contribute similar amounts of latent heat during the suppressed and active stages. This changing relationship between S-DCC and S-WCC contrasts the central Indian Ocean where heating from S-WCC always dominants heating from S-DCC. Additionally, the contribution from S-WCC maximizes during the transition stages in the West Pacific Ocean but maximizes during the active stage in the central Indian Ocean. The fact that the variability in heating from S-BSRs, S-WCCs, and S-DCCs differs in each geographic region is expected since Barnes and Houze [2013] demonstrated that the MJO modulates the areal coverage of BSRs, WCCs, and DCCs differently in these regions. Even though differences exist between the central Indian and West Pacific Oceans, our results indicate that the heating produced by S-BSR, S-WCC, and S-DCC account for a substantial amount of the net heating from S-All during the MJO in both regions, especially during the active stage.

6. Conclusions

Previous studies have used the TRMM PR to demonstrate that a transition from shallow to deep heating occurs as the MJO enters its active stage [e.g., Morita et al., 2006; Lin et al., 2004; Lau and Wu, 2010; Zuluaga et al., 2010; Jiang et al., 2011]. However, convection takes on different forms, with different heating profiles, in different large-scale environments, and the net heating profile affecting the large-scale dynamics depends on the particular mixture of types of convection making up the cloud population. By classifying individual storms in terms of their radar echo structure, the current study indicates how different forms of convection contribute to the latent heating observed during the MJO in the central Indian and West Pacific Oceans.

The classification technique that we have applied to the TRMM data is a proxy for the dynamical characteristics that produce different forms of convection, and it captures a significant amount of the latent heating variability associated with the variable makeup of the convective population of the MJO. Mature mesoscale systems containing broad expanses of stratiform precipitation are represented by an echo category referred to as storms with broad stratiform regions (S-BSR storms). Storms that have developed wide regions of intense convective echo but have not developed broad stratiform regions are identified as storms with wide convective cores (S-WCC storms). These storms are convective systems that have begun to organize on the mesoscale but not yet matured. Echoes containing deep convective cores but no wide convective regions or broad stratiform regions (S-DCC storms) are intense convection in an early stage of development. These interpretations of the radar echoes have been validated by ground-based radar data [Zuluaga and Houze, 2013].

TRMM PR echoes that do not meet the criteria of the above-described storm types are referred to as S-Non storms. They are often associated with convective echoes reaching midlevel top heights. Our analysis indicates that this S-Non convection is actually the greatest source of low-level heating during all stages of the MJO in both geographic regions—often outweighing heating by the more extreme forms of convection. However, it is well known that the SLH algorithm used in this study tends to produce more shallow heating than other TRMM algorithms and reanalysis [e.g., *Ling and Zhang*, 2011]. Thus, the magnitude of the S-Non heating may be somewhat exaggerated in this study. Additionally, while our results indicate that shallow isolate radar echoes (ISEs) contribute relatively little latent heat to the net heating budget, the TRMM PR data do not include all of the smaller convection because of the TRMM PR's rather high minimum detectable



reflectivity of ~17 dBZ. As a result, the TRMM data do not include nonprecipitating or lightly precipitating convection, which are likely important contributors to low-level heating in the MJO.

The greatest overall variability of the MJO heating profile in both geographic regions is due to the occurrence of S-BSR storms in active stages of the MJO and their relative absence in suppressed stages. This result is consistent with previous work showing that large, often merged MCSs are proportionately more prevalent in the active MJO stages [*Yuan and Houze*, 2010] and the tendency of large stratiform rain areas to occur mainly in the active stages [*Barnes and Houze*, 2013]. The more numerous occurrence of S-BSR storms during the active MJO stages leads to a top heavy heating profile that maximizes in the active stage.

The MJO heating profile exhibits regional differences, especially in terms of the heating from convective precipitation. First, while S-WCC always contributes more latent heat than S-DCC over the central Indian Ocean, S-WCC only contributes more heat than S-DCC during the transition stages in the West Pacific Ocean. During the suppressed and active stages in the West Pacific Ocean, S-WCC and S-DCC contribute approximately equal amounts of latent heat. Additionally, the transition to a deep heating profile during the active stage occurs differently in the central Indian and West Pacific Oceans. During all phases of the MJO, there is a peak in heating at the 2-3 km level due mainly to the S-Non (nonextreme) convection in both regions. However, the variability in the magnitude of this low-level peak differs between the regions. In the central Indian Ocean, the suppressed stage of the MJO is characterized by an abundance of shallow heating (due to S-Non convection) near 2 km. The heating profile during the active stage has two peaks, near 3 and 6 km. The magnitude of the low-level peak is substantially larger than the low-level peak observed during the suppressed stage and is likely associated with increased heating from convection of moderate depth. The upper level peak is associated with increased stratiform precipitation. In the West Pacific, the latent heating profile peaks at 3 and 6 km during all phases of the MJO. The magnitude of the 3 km peak does not vary greatly from one stage to the next. The beginning of the active stage is identifiable when the magnitude of the 6 km peak strongly increases, in association with an increase in stratiform precipitation. Finally, differences in the convective population also cause the heating profile during the two transition periods to differ. In the central Indian Ocean, greater heating is observed at all levels during the transition to the active stage than the transition to the suppressed stage. In the West Pacific Ocean, the magnitude of the low-level heating is similar during both transition periods, but the magnitude of the upper level heating is substantially larger during the transition to the suppressed stage than the transition to the active stage.

Thus, the regional similarities in the heating profiles during the MJO are attributable to the S-BSR storms, but regional differences in the heating profiles are due more to differences in how the convective components of the storms vary between the central Indian and West Pacific Oceans. This result is consistent with the conclusions of *Houze* [1989], who suggested that despite the rather universal similarity of stratiform heating profiles throughout the tropics, the regional variability of the net heating profiles is likely determined by differing behavior of the convective components of the heating from one region to another. Our results indicate that highly organized, mature convection (S-WCC) is often just as important, if not more important, to the latent heat budget as young deep convection (S-DCC). The younger deep convection, while impressively intense, is associated with heating that is never larger than, and generally smaller in comparison with, the more organized mesoscale convection. In addition, the moderate convective entities (S-Non) are found to be important contributors to the heating along with the extreme categories. While each of these categories of convective heating is important, they manifest differently in the two geographical regions considered here.

Our results highlight how the latent heating profile during the MJO in the central Indian and West Pacific Oceans is determined by the mixture of different types and forms of convection making up the cloud population. As global models become ever higher in resolution, these different types of convection will be representable, and observations such as those analyzed here will have important uses for model verification. The numerical simulations' ability to capture the structure and variability of heating associated with midlevel convection and the convective and stratiform portion of deep convection can be assessed, and a more detailed assessment of the possible sources of error will be possible. As latent heating variability is evaluated regionally, observed differences, such as those between the central Indian and West Pacific Oceans analyzed here, can be used to determine whether models can obtain these regional differences for the right physical reasons.



Acknowledgments

The authors would like to thank Stacy Brodzik for help processing the data and three anonymous reviewers who provided helpful criticism and suggestions. The data used in this study were acquired as part of the NASA's Earth System Division and archived and distributed by the Goddard Earth Sciences (GES) Data and Information Services Center (DISC) Distributed Active Archive Center (DAAC) at daac. gsfc.nasa.gov. This research was funded by the Department of Energy grant DE-SC0008452/ER-65460, National Science Foundation grants AGS-1059611 and AGS-1355567, and NASA PMM grant NHX13AG71G.

References

- Barnes, H. C., and R. A. Houze Jr. (2013), The precipitating cloud population of the Madden-Julian Oscillation over the Indian and west Pacific Oceans, J. Geophys. Res. Atmos., 118, 6996-7023, doi:10.1002/jgrd.50375.
- Fu, X., and B. Wang (2009), Critical roles of the stratiform rainfall in sustaining the Madden-Julian Oscillation: GCM experiments, J. Clim., 22(14), 3939-3959.
- Haertel, P. T., G. N. Kiladis, A. Denno, and T. M. Rickenbach (2008), Vertical-mode decompositions of 2-day waves and the Madden-Julian Oscillation, J. Atmos. Sci., 65(3), 813-833.
- Hagos, S., C. Zhang, W.-K. Tao, S. Lang, Y. N. Takayabu, S. Shige, M. Katsumata, B. Olsen, and T. L'Ecuyer (2010), Estimates of tropical diabatic heating profiles: Commonalities and uncertainties, J. Clim., 67(11), 542-558.
- Hartmann, D. L., H. H. Hendon, and R. A. Houze Jr. (1984), Some Implications of the mesoscale circulations in tropical cloud clusters from large-scale dynamics and climate, J. Atmos. Sci., 14(1), 113-121.
- Houze, R. A., Jr. (1982), Cloud clusters and large-scale vertical motions in the tropics, J. Meteorol, Soc. Jpn., 60(1), 396-410.
- Houze, R. A., Jr. (1989), Observed structure of mesoscale convective systems and implications for large-scale heating, Q. J. R. Meteorol. Soc., 115(487), 425-461.
- Houze, R. A., Jr. (2004), Mesoscale convective systems, Rev. Geophys., 42, RG4004, doi:10.1029/2004RG000150.
- Houze, R. A., Jr., D. C. Wilton, and B. F. Smull (2007), Monsoon convection in the Himalayan region as seen by the TRMM precipitation, Mon. Weather Rev., 133(627), 1389-1411.
- Jakob, C., and C. Schumacher (2008), Precipitation and latent heating characteristics of the major tropical western Pacific cloud regimes, J. Clim., 21(17), 4348-4364.
- Jiang, X., et al. (2011), Vertical diabatic heating structure of the MJO: Intercomparison between recent reanalysis and TRMM estimates, Mon. Weather Rev., 139(10), 3208-3223.
- Kerns, B. W., and S. S. Chen (2014), ECMWF and GFS model forecast verification during DYNAMO; Multiscale variability in MJO initiation over the equatorial Indian Ocean, J. Geophys. Res. Atmos., 119, 3736-3755, doi:10.1002/2013JD020833.
- Lappen, C.-L., and C. Schumacher (2012), Heating in the tropical atmosphere: What level of detail is critical for accurate MJO simulations in GCMs?, Clim. Dyn., 39(9-10), 3547-1368.
- Lau, K.-M., and H.-T. Wu (2010), Characteristics of precipitation, cloud, and latent heating associated with the Madden-Julian Oscillation, J. Clim., 23(3), 504-518.
- Li, C., X. Jia, J. Ling, W. Zhou, and C. Zhang (2009), Sensitivity of MJO simulations to diabatic heating profiles, Clim. Dyn., 32(2-3), 167-187. Lin, J., B. Mapes, M. Zhang, and M. Newmann (2004), Stratiform precipitation, vertical heating profiles, and the Madden-Julian Oscillation, J. Atmos. Sci., 61(3), 296-309.
- Ling, J. A., and C. D. Zhang (2011), Structural evolution in heating profiles of the MJO in global reanalyses and TRMM retrievals, J. Clim., 24(3), 825-842
- Ling, J., P. Bauer, P. Bechtold, A. Beljaars, R. Forbes, F. Vitart, M. Ulate, and C. D. Zhang (2014), Global versus local MJO forecasts skill of the ECMWF model during DYNAMO, Mon. Weather Rev., 142(6), 2228-2247.
- Madden, R. A., and P. R. Julian (1971), Detection of a 40-50 day oscillation in the zonal wind in the tropical Pacific, J. Atmos. Sci., 28(8), 702-708. Madden, R. A., and P. R. Julian (1972), Description of global-scale circulation cells in the tropics with a 40-50 day period, J. Atmos. Sci., 29(5), 1109-1123
- Maloney, E. D., and D. L. Hartmann (2000), Modulation of eastern North Pacific hurricanes by the Madden-Julian Oscillation, J. Clim., 13(9), 1451-1460.
- Morita, J., Y. N. Takayabu, S. Shige, and Y. Kodama (2006), Analysis of rainfall characteristics of the Madden-Julian Oscillation using TRMM satellite data, Dyn. Atmos. Oceans, 42, 107-126, doi:10.1016/j.dynatmoce.2006.02.002.
- Rasmussen, K. L., and R. A. Houze Jr. (2011), Orogenic convection in subtropical South America as seen by the TRMM PR, Mon. Weather Rev.,
- Romatschke, U., and R. A. Houze Jr. (2010). Extreme summer convection in South America, J. Clim., 23(14), 3761–3791.
- Romatschke, U., S. Medina, and R. A. Houze Jr. (2010), Regional, seasonal, and diurnal variations of extreme convection in the South Asian region, J. Clim., 23(2), 419-439.
- Roundy, P. E., C. J. Schreck, and M. A. Janiga (2009), Contributions of convectively coupled equatorial Rossby waves and Kelvin waves to the real-time multivariate MJO indices, Mon. Weather Rev., 137(1), 469-478.
- Schumacher, C., and R. A. Houze Jr. (2003), The TRMM Precipitation radar's view of shallow, isolated rain, J. Appl. Meteorol., 42(10), 1519–1524. Schumacher, C., R. A. Houze Jr., and I. Kraucunas (2004), The tropical dynamical response to latent heating estimates derived from the TRMM Precipitation Radar, J. Atmos. Sci., 61(12), 1341-1358.
- Shige, S., Y. N. Takayabu, W.-K. Tao, and D. E. Johnson (2004), Spectral retrieval of latent heating profiles from TRMM PR data. Part I: Development of a model-based algorithm, J. Appl. Meteorol., 43(8), 1095-1113.
- Shige, S., Y. N. Takayabu, W.-K. Tao, and C.-L. Shie (2007), Spectral retrieval of latent heating profiles from TRMM PR data. Part II: Algorithm improvement and heating estimates over tropical ocean regions, J. Appl. Meteorol., 46(7), 1098-1124.
- Shige, S., Y. N. Takayabu, S. Kida, W.-K. Tao, X. Zeng, C. Yokoyama, and T. L'Ecuyer (2009), Spectral retrieval of latent heating profiles from TRMM PR data. Part IV: Comparison of lookup tables from two- and three-dimensional cloud-resolving model simulations, J. Clim., 22(20),
- Slingo, J. M., et al. (1996), Intraseasonal oscillations in 15 atmospheric general circulation models: Results from an AMIP diagnostic subproject, Clim. Dvn., 12(5), 325-357.
- Stachnik, J. P., C. Schumacher, and P. E. Ciesielski (2013), Total heating characteristics of the ISCCP tropical and subtropical cloud regimes, J. Clim., 26(18), 7097-7116.
- Straub, K. (2013), MJO initiation in the real-time multivariate MJO index, J. Clim., 26(4), 1130-1151.
- Tao, W.-K., S. Lang, J. Simpson, and R. Adler (1993), Retrieval algorithms for estimating the vertical profiles of latent-heat release—Their applications from TRMM, J. Meteorol. Soc. Jpn., 71(6), 687-700.
- Tao, W.-K., et al. (2006), Retrieval of latent heating from TRMM measurements, Bull. Am. Meteorol. Soc., 87(11), 1555–1572.
- Tao, W.-K., S. Lang, X. P. Zeng, S. Shige, and Y. Takayabu (2010), Relating convective and stratiform rain to latent heating, J. Clim., 23(7), 1874–1893. Tokioka, T., K. Yamazaki, A. Kitoh, and T. Ose (1988), The equatorial 30-60 day oscillation and the Arakawa-Schubert penetrative cumulus parameterization, J. Meteorol. Soc. Jpn., 66(6), 883-901.
- Waliser, D. E. (2005), Predictability of tropical intraseasonal variability, in The Predictably of Weather and Climate, edited by T. Palmer and R. Hagedorn, pp. 275-305, Cambridge Acad. Press, Cambridge.



Journal of Geophysical Research: Atmospheres

- Waliser, D. E., et al. (2003), AGCM simulations of intraseasonal variability associated with the Asian summer monsoon, *Clim. Dyn.*, *21*(5–6), 423–446.
- Wang, B. (2005), Theory, in *Tropical Intraseasonal Oscillation in the Atmosphere and Ocean*, edited by W. K.-M. Lau and D. E. Waliser, pp. 307–351, Springer Praxis Publishing, U. K.
- Wheeler, M. C., and H. H. Hendon (2004), An all-season real-time multivariate MJO index: Development of an index for monitoring and prediction, *Mon. Weather Rev.*, 132(8), 1917–1932.
- Yuan, J., and R. A. Houze Jr. (2010), Global variability of mesoscale convective system anvil structure from A-train satellite data, *J. Clim.*, 23(21), 5864–5888.
- Zhang, C. (2005), Madden-Julian Oscillation, Rev. Geophys., 43, RG2003, doi:10.1029/2004RG000158.
- Zhang, C. (2013), Madden-Julian Oscillation: Bridging weather and climate, Bull. Am. Meteorol. Soc., 94(12), 1849–1870.
- Zhang, C. D., J. A. Ling, S. Hagos, W.-K. Tao, S. Lang, Y. N. Takayabu, S. Shige, M. Katsumata, W. S. Olson, and T. L'Ecuyer (2010), MJO signals in latent heating: Results from TRMM retrievals, *J. Atmos. Sci.*, 67(11), 3488–3508.
- Zhang, G. J., and M. Q. Mu (2005), Simulation of the Madden-Julian Oscillation in the NCAR CCM3 using a revised Zhang-McFarlane convection parameterization scheme, *J. Clim.*, 18(19), 4046–4064.
- Zuluaga, M. D., and R. A. Houze Jr. (2013), Evolution of the population of precipitating convective systems over the equatorial Indian Ocean in active phases of the Madden-Julian Oscillation, *J. Atmos. Sci.*, 70(9), 2713–2725.
- Zuluaga, M. D., C. D. Hoyos, and P. J. Webster (2010), Spatial and temporal distribution of latent heating in the South Asian Monsoon Region, *J. Clim.*, 23(8), 2010–2029.